Langmuir

Article

pubs.acs.org/Langmuir

Generating Singlet Oxygen Bubbles: A New Mechanism for Gas−Liquid Oxidations in Water

Dorota Bartusik,[†] David Aebisher,[†] BiBi Ghafari,[‡] Alan M. Lyons,*[,‡] and Alexander Greer*[,†]

[†]Department of Chemistry, Brooklyn College, City University of New York, Brooklyn, New York 11210, United States

[‡]Department of Chemistry, College of Staten Island, City University of New York, Staten Island, New York 10314, United States

Supporting Information

ABSTRACT: Laser-coupled microphotoreactors were developed to bubble singlet oxygen [$^1O_2$ ($^1\Delta_g$)] into an aqueous solution containing an oxidizable compound. The reactors consisted of custom-modified SMA fiberoptic receptacles loaded with 150 μm silicon phthalocyanine glass sensitizer particles, where the particles were isolated from direct contact with water by a membrane adhesively bonded to the bottom of each device. A tube fed O_2 gas to the reactor chambers. In the presence of O_2, singlet oxygen was generated by illuminating the sensitizer particles with 669 nm light from an optical fiber coupled to the top of the reactor. The generated $^1O_2$ was transported through the membrane by the O_2 stream and formed bubbles in solution. In solution, singlet oxygen reacted with probe compounds (9,10-anthracene dipropionate dianion, *trans*-2-methyl-2-pentanoate anion, *N*-benzoyl-D,L-methionine, or *N*-acetyl-D,L-methionine) to give oxidized products in two stages. The early stage was rapid and showed that $^1O_2$ transfer occurred via bubbles mainly in the bulk water solution. The later stage was slow; it arose only from $^1O_2$-probe molecule contact at the gas/liquid interface. A mechanism is proposed that involves $^1O_2$ mass transfer and solvation, where smaller bubbles provide better penetration of $^1O_2$ into the flowing stream due to higher surface-to-volume contact between the probe molecules and $^1O_2$.

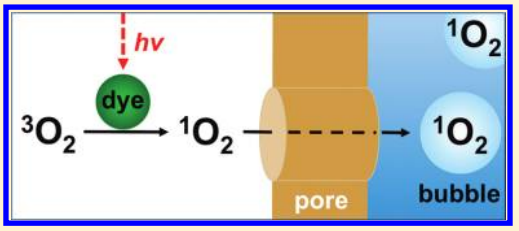

INTRODUCTION

Our interest in developing a singlet oxygen [$^1O_2$ ($^1\Delta_g$)]-sparging reactor came from small-scale devices for disinfection of, for example, municipal and well water, but which used filtration, ozone, and/or UV light.[1,2] Low-cost water purification inventions that use visible light to generate $^1O_2$ could be advantageous over ozone by using photocatalysts with high turnovers and over four decades of study of organic photooxidation product formation.[3,4] Photophysical information has been generated using visible light for the photosensitized disinfection of water samples or stagnating wounds,[5−8] but thus far, it is difficult to translate this information to handheld devices to deliver $^1O_2$ as a biological toxin via bubbles at the gas−liquid interface.

We[9−12] and others[13] have reported the $^1O_2$ production from hollow-tube configured devices. Our previous results established a singlet oxygen sensitization process with silica end-capped hollow-core fiber optic devices, utilizing the released $^1O_2$ for *Escherichia coli* inactivation[10] in a slow sparging system (9 ppm/h O_2). Eisenberg et al.[13] reported on a Pyrex tube bound Rose Bengal photosensitizer, surrounded by lamps, rapidly flowing $^3O_2$, $^1O_2$, and N_2 (30 L/min) in a gas−solid system. But unlike these previous systems, our desire was to produce singlet oxygen in a device that does not expose the photosensitizer to the water being purified. Since sensitizer molecules themselves may pose health risks, a means to isolate the sensitizer molecules from water was desired for water purification and/or applications where the device would come in contact with bodily fluids (e.g., surgery for cleansing and disinfecting wounds[8]).

One approach to increase the rate of singlet oxygen production is using chemical oxygen−iodine lasers (COIL).[14] These can produce gaseous $^1O_2$ bubbles up to supersonic speeds. COIL is not catalytic, but the ratio of $^1O_2$ to total oxygen concentrations is high, 30−50%, based on 2,5-dimethylfuran trapping studies.[15] However, this approach is problematic, as alkaline perhydroxyl ion (HO_2^-) and chlorine gas are required in high concentrations, several moles per liter of the former, and a few kilopascals pressure of the latter forming HCl as a byproduct.

As part of an ongoing study of handheld singlet oxygen $^1O_2$-generating devices,[9−12] we report here on a $^1O_2$ sparging device which used photosensitized phthalocyanine particles isolated from bulk water by a hydrophobic microporous membrane. Figure 1 shows a cross-sectional schematic image of the device (3 versions of which were constructed). Singlet oxygen was generated in the photoreactor and flowed through the membrane into the surrounding aqueous solution where it was detected, trapped, and analyzed. The sensitizer particles remain dry as the capillary pressure resulting from the submicrometer pores prevents water from diffusing through the membrane. Specifically, this paper describes (1) the use of Si phthalocyanine, axially functionalized via a sol−gel process as a

Received: November 21, 2011
Revised: December 21, 2011
Published: January 20, 2012

   dx.doi.org/10.1021/la204583v | *Langmuir* 2012, 28, 3053−3060

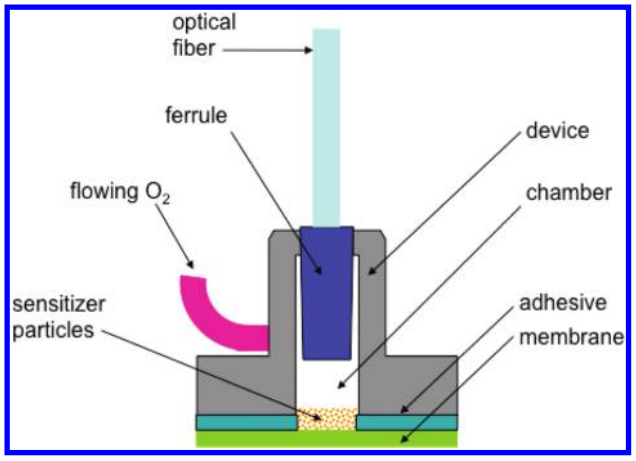

Figure 1. Geometry of the $^1O_2$-sparging photogenerator. At the top is the optical fiber leading from the diode laser, and at the left is the O_2 feed tube, connected to an oxygen gas tank. The lower part of the device, which contains a chamber for stockpiled silicon phthalocyanine sensitizer particles, was sealed with a microporous membrane.

heterogeneous photosensitizer; (2) device construction including membrane selection and attachment to a flexible optical fiber; (3) performance of the device to photooxidize probe compounds in water and the effects of bubble sizes; and (4) a proposed gas–liquid photooxidation mechanism via O_2 bubbles with mass transfer limitations.

EXPERIMENTAL SECTION

Reagents, Materials, and Instrumentation. Silicon phthalocyanine dichloride ($SiPcCl_2$), 3-aminopropyltriethoxysilane (ATPS), 3-glycidyloxypropyl-trimethoxysilane (GPTMS), 9,10-anthracene dipropionic acid, *trans*-2-methyl-2-pentenoic acid, *N*-benzoyl-D,L-methionine, *N*-acetyl-D,L-methionine, sodium hydroxide, hydrochloric acid, ethanol, methanol, deuterium oxide-d_2, and chloroform-d_1 were purchased from Sigma Aldrich (Allentown, PA). Deionized water was purified using a U.S. Filter Corporation deionization system (Vineland, NJ). All of the above materials and chemicals were used as received without further purification. The membranes were manufactured from ultrahigh molecular weight polyethylene (UHMWPE) and are composed of fibrils linked together to form a membrane of interpenetrating pores with a nominal pore area of 85% for each membrane (Millipore SureVent UPE Membranes, Billerica, MA). For the D_2O samples, proton NMR spectra were recorded at 400 MHz on Bruker DPX400 instrument. UV–vis spectra were collected on a Hitachi UV–vis U-2001 spectrophotometer.

Synthesis. The addition of $SiPcCl_2$ (5.1×10^{-4} M) to APTS (0.178 M) was conducted with stirring for 50 h at 120 °C, yielding an SiPc-APTS complex. The addition of GPTMS to the SiPc-APTS complex was carried out in acidic aqueous ethanol at 60 °C for 1 h; the temperature was then adjusted to 25 °C for 72 h, followed by drying at 50 °C for 10 h. The concentration of *Pc* within the gel corresponded to $\sim 5.2 \times 10^{-6}$ M based on UV–vis spectroscopy.

Devices and Procedure for Photooxidations. Optical energy was delivered from a CW diode laser (669 nm output, 506 mW, model 7404, Intense Ltd., North Brunswick, NJ, USA) or a Minilase 10 Hz Nd:YAG Q-switched laser (355 nm, ~4 ns fwhm, 1–3 mJ/pulse, New Wave Research, Fremont, CA) into a stainless steel multimode FT-400-EMT optical fiber with an SMA 905 connector (numerical aperture 0.39; 0.4 μm core diameter × 3 ft length, Thorlabs, Newton NJ). Ground *Pc* sensitizer particles were placed into the SMA receptacle chambers. The diode laser was used for the steady-state experiments with **2**–**5** (0.05 to 40 mM). The Nd:YAG laser was used for the lifetime measurements of singlet oxygen; it was connected to the optical fiber via a free-space PAF-SMA-5-A fiber port applicator (f = 4.6 mm). All experiments were conducted with the devices placed into 3.0 mL solutions of H_2O or D_2O and oxygen flowed through the devices and into the solutions during the irradiation of the samples. An H10330A-45 photomultiplier tube (Hamamatsu Corp., Hamamatsu City, Japan) was used operating at −650 V. In front of the A10449 mechanical shutter of the detector was placed either a 25-mm-diameter, 1150 nm long pass filter (FEL1150, Thorlabs Inc.) or one of three 25-mm-diameter NIR bandpass filters centered at 1220, 1270, and 1315 nm (OD4 blocking, fwhm = 15 nm, Omega, Brattleboro, VT). In D_2O, the $^1O_2$ luminescence intensity was measured to be 0.078 with the 1150 nm long pass filter, and 0.005, 0.08, and ~0 mV with the 1220, 1270, and 1315 nm bandpass filters, respectively; subtractions of the signals was not performed. Singlet oxygen was monitored based on the spectra consisting of ~1 million data points registered on a 600 MHz 62MXs-B oscilloscope (LeCroy, Chestnut Ridge, NY). The singlet oxygen decay lifetime was determined by nonlinear least-squares curve-fitting with the equation: $\text{luminescence}_{1270}(t) = A \times [\exp^{-(t/\tau)}]$, where $1/k_{obs} = \tau(^1O_2)$ lifetime. The data processing was performed with Microsoft *Excel* (v 12.3.1). The radiant power of the 355 nm and 669 nm light exiting the fiber or devices 1–3 was measured with a Newport power meter model 1918-C. Some of the laser light encountered the bubbles and was scattered. The bonded membranes were susceptible to aging after prolonged exposure times (e.g., >100 h with device 1 loaded with 35 mg sensitizer particles) and led to increased membrane elasticity and increased laser power output measured outside of the membrane by ~10% from 0.098 to 0.11. Careful inspection of the water samples after photolysis showed that no sensitizer particles had escaped the device so that the observed photooxidation could not be due to sensitizer particles within the water. Gas flowed from a compressed oxygen gas tank through a regulator, and subsequently a mass flow controller (GFC-17, Aalborg, Orangeburg, NY). The concentration of O_2 in water was measured with a pO_2 Sens-Ion6 oxygen electrode (Hach Co., Loveland, CO).

RESULTS AND DISCUSSION

Photosensitizer Synthesis. It was desirable to use a heterogeneous sensitizer with a strong absorption in the 670 nm region to match the 669 nm output of our diode laser. Si phthalocyanine (*Pc*) was selected because it possessed a strong absorption in the red spectral region (extinction coefficients $>10^5$ M^{-1} cm^{-1}), and the $^1O_2$ quantum yield (Φ_Δ) was reported to be ~0.2.[16,17]

Composite (*Pc* **1**) was prepared by a sol–gel process using a previously described procedure except with relatively low concentrations of *Pc*.[18] Silicon *Pc* dichloride ($SiPcCl_2$) reacted with 3-aminopropyltriethoxysilane [$(NH_2(CH_2)_3Si(OC_2H_5)_3$, APTS] in a 1:350 molar ratio at 120 °C producing SiPc $[NH(CH_2)_3Si(OC_2H_5)_3]_2$, which reacted with 3-glycidyloxypropyl-trimethoxysilane (GPTMS) to produce *Pc* **1**, which contained an assortment of bonds cross-linked, such as Si–O–Si bonds from condensation, and polyether chains and dioxane rings via epoxide ring-opening reactions.[19] Drying of the composite was done at 50 °C for 10 h to avoid destruction of the confined phthalocyanine molecules, producing an aerogel that shrunk ~10% where some, but not all adsorbed water was removed. Complete dehydration occurs between 100 and 180 °C.[20] Low final *Pc* concentrations in the glass ($\sim 5.2 \times 10^{-6}$ M) were targeted because dye overloading or crowding can lower $^1O_2$ yields.[21,22] *Pc* **1** was ground and sieved to obtain 150 ± 30 μm sized particles. The surface area of each 150 μm *Pc* **1** sensitizer particle was approximately 0.06971 mm^2, based on the calculations of Skidmore and Powers,[23] assuming a spherical nonporous surface. Spectroscopically, *Pc* **1** contained the desired 670 nm Q-band for overlap with the diode laser excitation wavelength and the lack of a red-shifted absorption expected of monomeric *Pc* in the glassy matrix.

dx.doi.org/10.1021/la204583v | *Langmuir* 2012, 28, 3053–3060

Device Construction. Devices were constructed to isolate the solid *Pc* **1** sensitizer particles from the surrounding water solution with an "internal" supply of light and flowing O_2. A chamber within each device functioned as a reactor for the sensitizer particles, light, and O_2, to generate $^1O_2$.

Figure S4 (Supporting Information) shows the loading of device 2 with sensitizer particles, as well as the three devices without the optical fibers attached. Each device was fabricated from a chrome-plated brass SMA receptacle with a SMA connector at one end of a cylindrical chamber (Amphenol). The dimensions of the chamber, and other device details, are listed in Table S1 (Supporting Information). Because device 3 was larger, the mg of *Pc* **1** particles that could be loaded into it was 740 mg, whereas devices 1 and 2 could only hold 75 mg. Table S2 shows the estimated total surface area of the particles and the number of particles that can be loaded into the devices. The term surface area refers only to the exterior surface area of the particle and does not consider internal pores. It is known that sol−gel glasses can be highly porous.[24] The diode laser was connected by attaching the fiber SMA fitting to the device. The divergence angle of the red light exiting the fiber was not matched to the membrane area. The opposite, open end was sealed with the porous membrane. A hole was drilled into the cavity and a brass tube, 1/16 in. o.d., was soldered in place to introduce the oxygen feed gas supply between the laser and the sensitizer.

Devices were fabricated with membranes of different pore sizes and thicknesses (Millipore). The membranes were manufactured from ultrahigh molecular weight polyethylene (UHMWPE) and are composed of fibrils linked together to form a membrane of interpenetrating pores with a nominal pore area of 85% for each membrane. UHMWPE is biocompatible and used extensively for medical implants. The membranes were adhesively bonded to the bottom surface of the receptacle using a 3 M pressure sensitive tape coated on both surfaces with a high bond strength adhesive. The pressure sensitive tape was die cut to form a ∼5 mm hole to allow the sensitizer to sit directly onto the membrane.

To ensure that liquid does not penetrate the membrane and interact with the sensitizer, the membranes were selected such that the capillary pressure was sufficiently high to exclude water. The capillary pressure was calculated from the Young−Laplace equation:

$$p_c = \frac{2\gamma \cos\theta}{r} \quad (1)$$

where p_c is the capillary pressure, γ is the liquid surface tension, θ is the contact angle between the liquid and the membrane material, and r is the pore radius. For water and UHMWPE, the values of γ and θ are 72 dyn/cm and 105°, respectively. Thus, the capillary pressure will be inversely proportional to the pore radius; the larger the radius, the lower the pressure. Supporting Information Table S1 shows that decreasing the diameter of the pores in the membrane increased the capillary pressure and so keeps water from infiltrating the membrane at higher pressures. For example, the capillary pressure of a 0.44 μm pore is 12 psi, whereas the capillary pressure of a 0.05 μm pore is 108 psi. Thus, the device with a 0.44 μm pore membrane could be submerged to a depth of ∼8 m of water before water ingress could occur, whereas the 0.05 μm pore membrane would prevent ingress at depths over 75 m of water. In our experiments, no leaching of sensitizer was observed with any device, regardless of membrane pore size (see Experimental Section). For the membranes studied, the capillary pressure values range from 75×10^4 to 8.5×10^4 Pa (108−12 psi, as noted above). Thinner membranes with smaller pore diameters are also advantageous as the reduced thickness shortens the path over which $^1O_2$ must diffuse before contacting water or being detected. However, the thinner membranes are somewhat fragile and may create a greater pressure drop for gas flow. Thicker membranes with larger pores are more robust.

Device Operation. The effect of membrane pore size and of sensitizer particle loading on the size of bubbles exiting the devices is shown in Table 1. The *Pc* particles tended to pool in the center of the membrane where it bulged from the O_2 pressure. Individual bubbles ranged in diameter from 2 to 10 mm, where their sizes decreased with smaller membrane pores, in the order 0.05 μm < 0.22 μm < 0.44 μm. Higher loadings of sensitizer particles in the devices also led to smaller bubbles. Table 2 shows the volume and number of bubbles transmitted per experiment. Bubbles were mostly cylindrical and monodisperse, although some bubble clustering occurred, the bubble coalescence behavior at the membrane/water interface was not scrutinized. The 0.091, 0.14, and 0.46 mL bubbles that emerged from devices 1, 2, and 3, respectively, provided agitation to the solution (Figure 2).

Table 1. Bubble Sizes Egressing into Aqueous Solution, and Power Measurements

device number	membrane pore size (μm)	quantity of *Pc* **1** loaded into devices (mg)	bubble diameter (mm)[a,b]	power (mW) measured outside of the membrane[c]
1	0.05	0	∼5	3.5
		1	∼4.8	2.9
		3	4.2 ± 0.8	2.5
		10	3.6 ± 0.5	0.15
		35	2.8 ± 0.4	0.098
		50	2.8 ± 0.4	0.0076
		75	∼2	0.0085
2	0.22	0	∼5	2.5
		1	∼5	2.0
		3	∼4	1.5
		10	3.4 ± 0.5	0.76
		35	3.2 ± 0.4	0.16
		50	∼3	0.0075
		75	∼2	0.0060
3	0.44	0	∼10	5.0
		1	7.6 ± 1.5	3.0
		3	7.4 ± 1.8	2.7
		10	5.8 ± 1.1	1.5
		35	4.8 ± 1.3	0.14
		50	4.6 ± 0.9	0.0089
		75	4.2 ± 0.8	0.010

[a]The bubble sizes effusing through the device membranes were measured from photographic images with ruler reference points and/or pixel size correlations. The values shown here are averages of 2 or more measurements. [b]The experiments were carried out flowing O_2 at a rate of 60 mL/min with a regulator pressure of 35 psi and a ∼2 mm height of water above the membrane. [c]The output of the diode laser (669 nm, 506 mW) was coupled to the fiber optic, where 383 mW laser light exited the fiber optic and entered the top portion of the devices at the fiber optic/SMA junction.

With the diode laser turned off, no apparent cooling of the aqueous solution occurred from the devices sparging O_2 at a

dx.doi.org/10.1021/la204583v | *Langmuir* 2012, 28, 3053−3060

Table 2. Effect of Membrane Pore Size on Bubble Volume and Number Transmitted[a]

device number	sensitizer **1** loaded into device (mg)	membrane pore size (μm)	bubble volume (mL)	number of bubbles transmitted[b]
1	35	0.05	0.091	98 900
2	35	0.22	0.14	65 700
3	35	0.44	0.46	19 400

[a]Devices were loaded with 0.35 mg *Pc* **1**; O_2 flow rate was 60 mL/min; solution was 3 mL D_2O. [b]Over the course of a 2.5 h experiment, 9 L of O_2 was consumed.

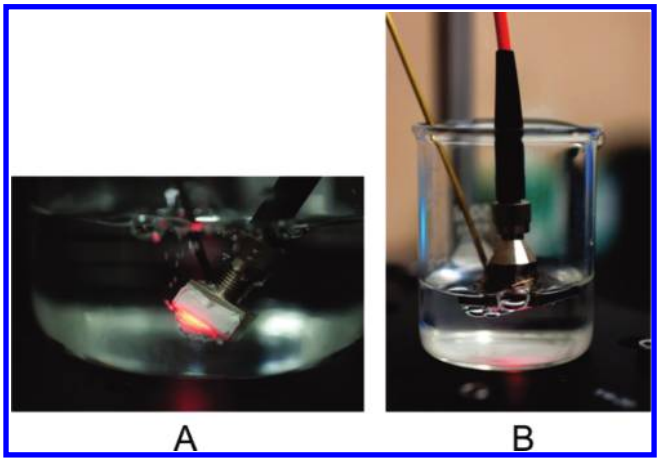

Figure 2. (A) Device 1, with smaller pores than the other two devices, is seen here. It shows $^1O_2$ bubbling from the distal end of the device. The membrane bulges due to oxygen pressure during the irradiation. The side and bottom were covered with the 0.05 μm membrane to improve adhesion. (B) Device 3 attached to the 0.44 μm membrane. At the bottom, relatively larger O_2 bubbles can be seen emerging from the membrane. The larger bubbles result in smaller surface-to-volume ratios and limited $^1O_2$ contact, which may explain why this device was less efficient in oxidizing compounds in the surrounding water solution.

rate of 60 mL/min. In contrast, with the diode laser turned on, the solution temperature increased from 22 to 28 °C. We measured only a very small light output through the membrane (0.006–0.010 mW when loaded with sensitizer and 2.0–5.0 mW with no sensitizer) and so we estimated that most of the light (~380 mW) was absorbed by the sensitizer particles and walls of the device, which subsequently transferred the heat to the solution in which it was immersed. There was some variability of light absorption in the devices, resulting from the different chamber sizes. Oxygen solubility is reported to decrease from 7.9 ppm O_2 at 25 °C to 7.2 ppm O_2 at 30 °C and its mass transfer coefficient increases.[25]

Effect of Device Geometry and Bubble Size on Product Yield. Chemical trapping of $^1O_2$ was conducted in the surrounding aqueous solution with 9,10-anthracene dipropionate dianion (**2**), *trans*-2-methyl-2-pentenoic acid (**3**), *N*-benzoyl-D,L-methionine (**4**), and *N*-acetyl-D,L-methionine (**5**) (Figure 3).[9,26–32]

Devices 1–3 were connected to the 669 nm diode laser (fluence = 4128 J/cm^2) via an optical fiber and an O_2 gas tank (60 mL/min flow). Compounds **2**–**5** were photooxidized in 3.0 mL H_2O or D_2O downstream. Compounds **2** and **3** are specific quenchers of singlet oxygen, but **4** and **5** are not. The formation of 9,10-anthracene-9,10-endoperoxide dipropionate dianion (**6**) took place via a [4 + 2] cycloaddition of singlet oxygen with **2** (0.001 M, pH = 10), and the formation of

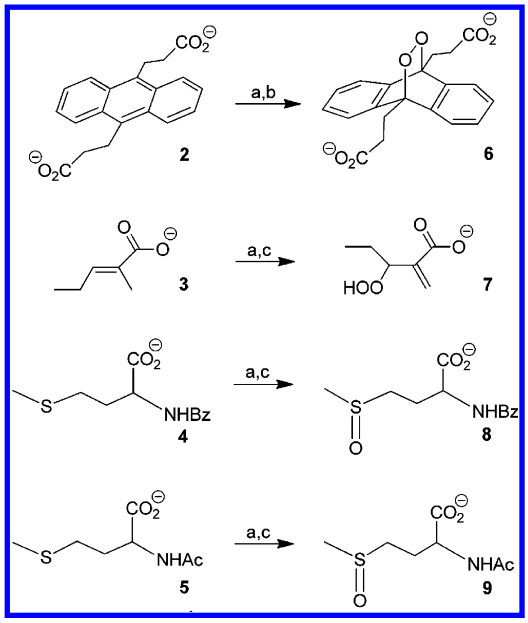

Figure 3. Chemical agents used to trap $^1O_2$ using (a) devices 1, 2, or 3; (b) in H_2O or D_2O; and (c) in D_2O.

3-hydroperoxy-2-methylene pentanoate anion (**7**) occurred via an "ene" reaction of singlet oxygen with **3** (0.04 M, pH = 10). Two moles of methionine sulfoxide formed per mole $^1O_2$ in the reaction of the corresponding methionines (**4** and **5**) (ea. 0.04 M, pH = 10). For the methionines **4** and **5**, the *S*-oxide products were detected, but not the sulfones or rearranged products, as seen in some mechanistic studies.[33,34] Because the $^1O_2$ lifetime is longer in D_2O (τ_Δ = 65 μs) than in H_2O (τ_Δ = 3.5 μs),[35] the preferred use of D_2O in the experiments in Table 3 was the result of shorter reaction times. Irradiation of **2**–**5** in the absence of sensitizer particles produced no products with all devices (cf. entry 1, 8, and 15).

As shown in Table 3, higher photooxidation yields were observed from smaller bubbles. We attributed this to the enhanced contact between trap molecule and $^1O_2$ due to higher surface-to-volume ratios resulting from smaller bubbles. Irradiation of **2** (1.0 mM) for 2.5 h led to 0.99, 0.42, and 0 μmol of endoperoxide **6** with devices 1, 2, and 3, respectively, each loaded with 35 mg of *Pc* **1** particles where bubble diameters were 2.8, 3.2, and 4.8 mm, respectively, as shown in Table 3.

Higher loadings of sensitizer particles also led to increased formation of products **6**–**9** likely due to an increase in exposed sensitizer surface area within the reactor chamber. In the case of 75 mg particle loading, the reaction yielded 1.38, 0.78, and 0.96 μmol of endoperoxide **6**. For all devices, a minimum quantity of sensitizer was required before photooxidized products could be detected; for devices 1 and 2, greater than 10 mg of sensitizer particles was required, for device 3, 35 mg was required.

Regarding the photoreactor design, it is important to note that melting of the sensitizer occurred when the laser-head was in close proximity to the particles. Since the melting point of *Pc* **1** is 65 °C, the temperature of the sensitizer was >25 °C. Thus, it was advantageous to use reduced loadings (e.g., 35 mg loadings) to increase the distance between the laser-head and the sensitizer particles to prevent excess heating of the sensitizer. On the other hand, the reduced product yields, compared to 75 mg loadings, was a disadvantage (Table 3).

Mechanism of Singlet Oxygen Mass Transfer. The formation of $^1O_2$ was further examined with device 1 loaded

dx.doi.org/10.1021/la204583v | *Langmuir* 2012, 28, 3053–3060

Table 3. Photooxidation of Probe Compounds in D_2O[a,b]

device number	entry	sensitizer particles loaded into device (mg)	yield of endoperoxide **6**, μmol (and %)[c]	yield of hydroperoxide **7**, μmol (and %)[d]	yield of benzoyl methionine *S*-oxide **8**, μmol (and %)[d]	yield of acetyl methionine *S*-oxide **9**, μmol (and %)[d]
1	1	0	0	0	0	0
	2	1	0	0	0	0
	3	3	0	0	0	0
	4	10	0	0	0.48 (0.8%)	1.14 (1.9%)
	5	35	0.99 (33%)	2.16 (1.8%)	1.74 (2.9%)	1.38 (2.3%)
	6	50	1.23 (41%)	4.68 (3.9%)	2.82 (4.7%)	2.16 (3.6%)
	7	75	1.38 (46%)	5.76 (4.8%)	4.50 (7.5%)	2.70 (4.5%)
2	8	0	0	0	0	0
	9	1	0	0	0	0
	10	3	0	0	0	0
	11	10	0.12 (4.0%)	0	0	0.6 (1.0%)
	12	35	0.42 (14%)	1.80 (1.5%)	0.66 (1.1%)	0.96 (1.6%)
	13	50	0.69 (23%)	3.84 (3.2%)	1.02 (1.7%)	1.35 (2.7%)
	14	75	0.78 (26%)	4.20 (3.5%)	1.55 (3.1%)	1.60 (3.2%)
3	15	0	0	0	0	0
	16	1	0	0	0	0
	17	3	0	0	0	0
	18	10	0	0	0	0
	19	35	0	1.20 (1.0%)	0.42 (0.7%)	0
	20	50	0.72 (24%)	1.80 (1.5%)	0.72 (1.2%)	0.60 (1.0%)
	21	75	0.96 (32%)	4.50 (2.5%)	1.44 (2.4%)	1.20 (2.0%)

[a]All samples were illuminated at 669 nm (fluence = 4128 J/cm^2) under an O_2 flow rate of 60 mL/min for 2.5 h at 28 °C. Over the course of each experiment 9 L of O_2 was consumed. [b]The concentrations of 3-hydroperoxy-2-methylene pentanoate anion **7**, *N*-benzoy-D,L-methionine *S*-oxide **8**, and *N*-acetyl-D,L-methionine *S*-oxide **9** were determined by ^{1}H NMR by the appearance of singlets at 2.71 ppm (s, 3H), at 5.56 ppm (s, 1H), and at 5.94 ppm (s, 1H), respectively. The concentration of endoperoxide **6** was estimated by UV−vis by the disappearance of the 9,10-anthracene dipropionate dianion **2** absorption at 378 nm. [c]The starting concentration of **2** was 1 mM (0.003 mmol). [d]The starting concentrations of **3**-**5** was 0.04 M (0.12 mmol).

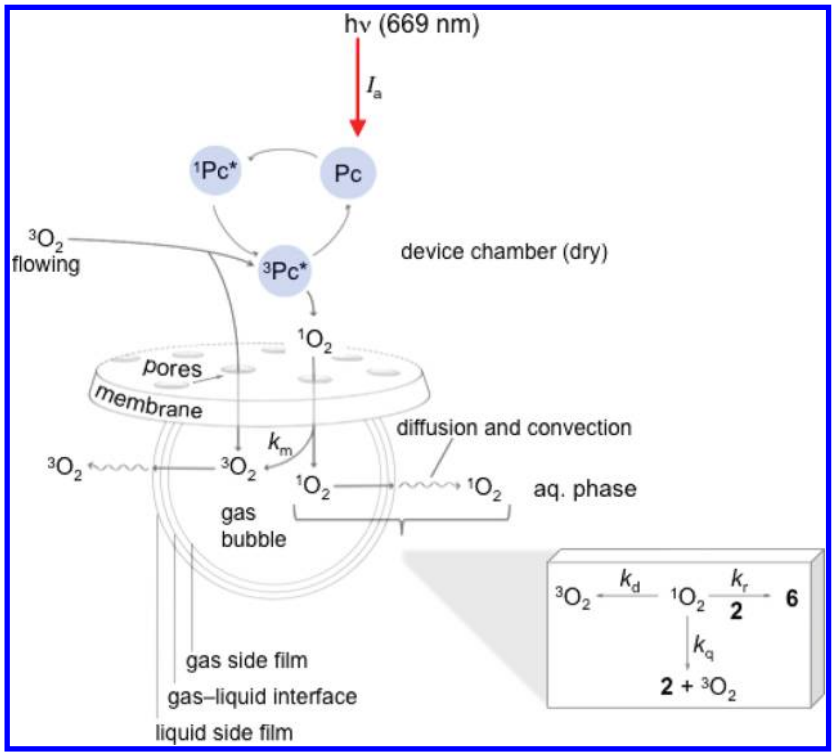

Figure 4. Proposed photooxidation mechanism.

with 35 mg sensitizer particles in H_2O and D_2O. The data are consistent with the mechanism in Figure 4, where I_a is the rate of light absorption by the *Pc* **1** particles, k_m is the device membrane deactivation rate constant, k_r is the trapping rate constant, k_q is physical quenching rate constant by the trapping agent, k_d is the decay rate constant by H_2O or D_2O. In H_2O, the O_2 concentration measured at t = 0 min was 1.5×10^{-4} M (4.7 ppm), according to a Clarke type oxygen electrode. Upon

dx.doi.org/10.1021/la204583v | *Langmuir* 2012, 28, 3053−3060

sparging O_2 via device 1, successive readings of O_2 concentrations were constant after 40 min when oxygen saturation was reached 8.3×10^{-4} M (26.6 ppm) (Figure 5).

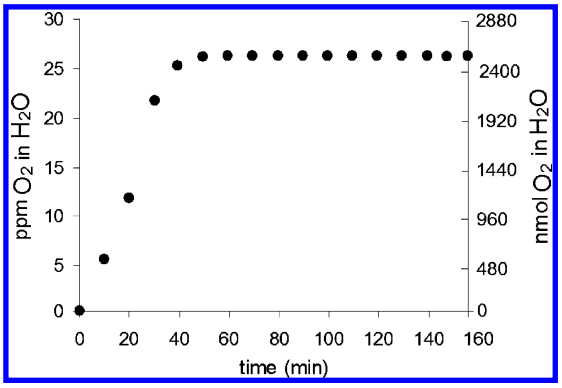

Figure 5. Solubility of O_2 in 3 mL H_2O as a function of time using device 1 loaded with 0.35 mg sensitizer particles. The flow rate was 60 mL/min.

We initially thought that oxygen would saturate this volume more quickly than 40 min, but the effect is likely due to the small bubbles generated from device 1.

Evidence suggested that $^1O_2$ transfer occurred via bubbles into bulk water prior to oxygen saturation of the solution. First, by monitoring the emission at 1270 nm, the lifetime of $^1O_2$ sparged into D_2O was found to be 60 ± 3 μs, which matched the value expected of $^1O_2$ in bulk D_2O, but increased to ~1 ms in air (Figure S7, Supporting Information). Second, rapid photooxidation of anthracene **2** was observed prior to O_2 saturation (0–40 min, Figure 6). The starting concentration of

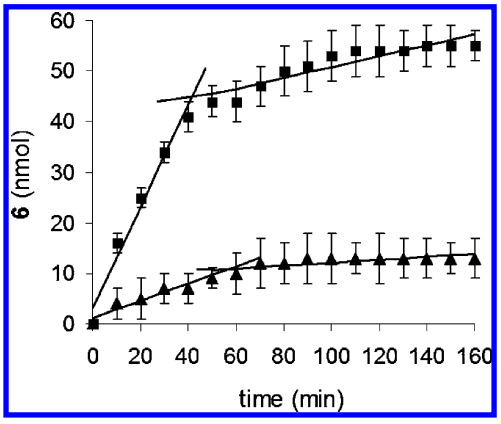

Figure 6. Nanomoles of photoproduct **6** as a function of time from device 1 loaded with 0.35 mg sensitizer particles with an O_2 flow rate was 60 mL/min into 3 mL D_2O (■) and H_2O (▲). The starting concentration of **2** was 0.05 mM (150 nmol **2**).

2 was 0.05 mM (150 nmol **2**). Lines were fitted to the fast stage of the plot, where the rate of formation of **6** was 1.1 nmol/min in D_2O and 0.2 nmol/min in H_2O from 0 to 40 min.

After the solution was saturated with O_2, the sensitivity of the slope reduced by 10-fold. This slower stage for the photooxidation of **2** might arise from contact of singlet oxygen and **2** at the gas–liquid interface with reduced $^1O_2$ transfer into bulk solution due to the O_2 equilibrium reached between the gas and liquid phases. The rate of formation of **6** was 0.12 nmol/min in D_2O and 0.02 nmol/min in H_2O from the period of ~40 to 160 min. After 160 min, 34% conversion of **2** was reached in D_2O. Control experiments showed that D_2O was saturated with O_2 about 2 times more rapidly than H_2O, and the solubility was slightly greater (cf. 32.5 ppm in D_2O with 26.6 ppm in H_2O). These two facets can help explain why the inflection point in Figure 6 occurs at about 40 min in D_2O and 60 min in H_2O.

We believe that singlet oxygen continues to transfer into the bulk water even after saturation. The water may saturate with O_2, but it is not static. O_2 would be vaporizing from the surface (at both the bulk liquid–air interface as well as liquid bubble interface), and new $^1O_2$ and O_2 would dissolve to replace, but the rate will be lower than before saturation. There is ample precedent that when an O_2 equilibrium exists in the gas and liquid phases O_2 exchange still occurs, concentrations of O_2 are linearly related in both phases (Henry's Law), but there is no net change in O_2 concentration, which is driven by a concentration gradient (Fick's Law).[36] There is a large amount of literature on how gas in bubbles interacts with aqueous solutions.[37] However, the two stages of the reaction indicate that the movement of the probe molecules in solution (convection) was caused by the bubbles overcoming the threshold quantity of product yields imposed by equilibrium.

The sensitivity of the slope of product formation in D_2O compared to H_2O prior to or after O_2 saturation of the solution was consistent with the longer lifetime of $^1O_2$ in the former.[35] Table 4 shows the ratio of endoperoxide **6** molecules formed

Table 4. Membrane Pore Sizes, Ratio of Oxygen Transmitted to Endoperoxide 6 Formed[a,b]

device number[c]	membrane pore size (μm)	ratio of endoperoxide **6** molecules to $^3O_2$ transmitted (ppm)	nanomoles **6** formed per sensitizer particle[d]
1	0.05	2.6	67
2	0.22	1.1	41
3	0.44	<0.1	<5

[a]Devices were loaded with 0.35 mg *Pc* **1**; O_2 flow rate was 60 mL/min; solution was 3 mL D_2O. The starting concentration of **2** was 1.0 mM (3 μmol **2**). [b]Over the course of experiment 9 L of O_2 was consumed. [c]Number of bubbles transmitted over the course of the experiment: 98 900 (device 1); 65 700 (device 2); 19 400 (device 3). [d]150 ± 30 μm sensitizer particles; 2.5 h reaction time.

to $^3O_2$ molecules transmitted, which translates (roughly) to the number of oxidized molecules that arose from each sensitizer particle. A lower limit of the number of $^1O_2$ molecules within the bubbles was ~3 ppm for device 1, ~2 ppm for device 2, and ≪1 ppm for device 3. Averaged over 2.5 h, the rate of **6** formation was ~8 nmol/min for device 1, ~4 nmol/min for device 2, and for device 3, no product was detected. The nanomole per minute rates we observe are about 100-fold less efficient than photooxidation batch reactors,[38–40] but for the batch reactors, the photosensitizer must be soluble in solution and then separated (e.g., via permeation chromatography). In contrast, our devices use a membrane, which effectively keeps the sensitizer dry and separated from the solution, and so there, is no concern with sensitizer removal after the reaction. Interest has surrounded the quenching of photosensitizers by O_2 at solution/solid and gas/solid interfaces[41–46] for clean external production of $^1O_2$,[47] and improved $^1O_2$ transmission would be conceivable in device membranes containing C–D or C–F bonds, since C–H bonds are more effective in the vibrational deactivation of $^1O_2$ in small organic molecules.[48,49] Isolating the photosensitizer from the solution avoids the possibility of

dx.doi.org/10.1021/la204583v | *Langmuir* 2012, 28, 3053–3060

ground-state hydrogen abstraction or electron transfer Type I photooxidation processes[4] for clean transmission of $^1O_2$ across the membrane.

We believe that the $^1O_2$ yield is significantly greater than the measured yield of oxidized acceptors. For the $^1O_2$ that was transported across the membrane, some $^1O_2$ was lost to other quenching processes, but the measured yield was severely limited by mass transport[50] across the membrane as well as into the solution. This results in much of the $^1O_2$ being released to the air when bubbles reach the bulk liquid−air interface, as shown in Figure S8, which has been recognized previously;[51] thus, the device appears to operate within gas−water mass transfer limitations.

CONCLUSION

We report on the fabrication and properties of a singlet oxygen-generating device, in which a solid *Pc* photosensitizer was isolated from an aqueous solution by using a porous membrane in a laser-coupled device. A sol−gel technique was used to synthesize the *Pc* photocatalyst within a glass matrix. Due to the high capillary pressure of the membrane, the sensitizer remains dry within the device as it is irradiated with laser light in the presence of an oxygen flow. Within the device, O_2 was sensitized by excited *Pc* sites in the particles. Singlet oxygen molecules were then transported across the membrane, forming bubbles at the membrane−water interface.

Not only do the smaller diameter pores in the membrane prevent water ingress at higher pressures, but the smaller pores also generate smaller bubbles and thus increase the device efficiency. Reaction rates between singlet oxygen and four probe compounds were measured and the rates were proportional to sensitizer particle loading and inversely proportional to the membrane pore diameter. Bubble diameter was correlated to pore diameter, and rates increased when smaller bubbles were observed. A mechanism is proposed whereby the oxidation of probe compounds is limited by transport of $^1O_2$ across the bubble−liquid interface. Given that flow is held constant in all experiments, smaller bubble diameters result in larger oxygen−water interfacial areas. In addition, the reaction rate slows by a factor of ∼10 after the solution becomes saturated with O_2. Oxygen saturation reduces the rate of $^1O_2$ transport from the bubble into the solution.

Water purification and wound disinfection are our long-term goals, and the first step in this paper was to demonstrate $^1O_2$ delivery from a photosensitizer isolated from water. Future experiments are planned, including evaluation of the effectiveness of the technique for inactivation of bacteria and oxidation of groundwater contaminants.

ASSOCIATED CONTENT

Supporting Information

Fluorescence and UV−vis spectra of *Pc* **1**, images of the SMA receptacle, photomicrographs of the membranes, luminescence signal of singlet oxygen in D_2O and in air, and an image of the loss of singlet oxygen in bubbles that reach the air interface. This material is available free of charge via the Internet at http://pubs.acs.org/.

AUTHOR INFORMATION

Corresponding Author

*E-mail: alan.lyons@csi.cuny.edu; agreer@brooklyn.cuny.edu.

ACKNOWLEDGMENTS

D.B., D.A., and A.G. acknowledge support from the National Institute of General Medical Sciences (NIH SC1GM093830). A.M.L. acknowledges support from the NYS Empire State Development's Division of Science, Technology & Innovation (NYSTAR). B.G. acknowledges support from the National Science Foundation STEM Talent Expansion via Applied Mathematics (STEAM) (Grant #0653056). We also thank Alison Domzalski for the photography work and Leda Lee for the graphic arts work. This paper is dedicated to the memory of Prof. Ronald Bentley of the University of Pittsburgh.

REFERENCES

(1) Gavasci, R.; Chiavola, A.; Spizzirri, M. *Water Sci. Technol.* **2010**, *62*, 1371−1378.
(2) Loeb, B. L. *Ozone: Sci. Eng.* **2011**, *33*, 329−342.
(3) Foote, C. S. *Acc. Chem. Res.* **1968**, *1*, 104−110.
(4) Greer, A. *Acc. Chem. Res.* **2006**, *39*, 797−804.
(5) Manjón, F.; Villén, L.; García-Fresnadillo, D.; Orellana, G. *Environ. Sci. Technol.* **2008**, *42*, 301−307.
(6) Benabbou, A. K.; Guillard, C.; Pigeot-Rémy, S.; Cantau, C.; Pigot, T.; Lejeune, P.; Derriche, Z.; Lacombe, S. *J. Photochem. Photobiol. A: Chem.* **2011**, *219*, 101−108.
(7) Remucal, C. K.; McNeill, K. *Environ. Sci. Technol.* **2011**, *45*, 5230−5237.
(8) Kammerlander, G.; Assadian, O.; Eberlein, T.; Zweitmuller, P.; Luchsinger, S.; Andriessen, A. *J. Wound Care* **2011**, *20*, 149−158.
(9) Zamadar, M.; Aebisher, D.; Greer, A. *J. Phys. Chem. B* **2009**, *113*, 15803−15806.
(10) Aebisher, D.; Zamadar, M.; Mahendran, A.; Ghosh, G.; McEntee, C.; Greer, A. *Photochem. Photobiol.* **2010**, *86*, 890−894.
(11) Mahendran, A.; Kopkalli, Y.; Ghosh, G.; Ghogare, A.; Minnis, M.; Kruft, B. I.; Zamadar, M.; Aebisher, D.; Davenport, L.; Greer, A. *Photochem. Photobiol.* **2011**, *87*, 1330−1337.
(12) Zamadar, M.; Ghosh, G.; Mahendran, A.; Minnis, M.; Kruft, B. I.; Ghogare, A.; Aebisher, D.; Greer, A. *J. Am. Chem. Soc.* **2011**, *133*, 7882−7891.
(13) Eisenberg, W. C.; Taylor, K.; Murray, R. W. *J. Phys. Chem.* **1986**, *90*, 1945−1948.
(14) Nikolaev, V. D.; Svistun, M. I.; Zagidullin, M. V.; Hager, G. D. *Appl. Phys. Lett.* **2003**, *86*, 231102.
(15) Spalek, O.; Kodymová, J.; Hirsl, A. *J. Appl. Phys.* **1987**, *62*, 2208−2211.
(16) Aoudia, M.; Cheng, G.; Kennedy, V. O.; Kenney, M. E.; Rodgers, M. A. J. *J. Am. Chem. Soc.* **1997**, *119*, 6029−6039.
(17) Rodríguez-Córdoba, W.; Noria, R.; Guarín, C. A.; Peon, J. *J. Am. Chem. Soc.* **2011**, *133*, 4698−4701.
(18) Xia, H.; Nogami, M.; Hayakawa, T.; Imazumi, D. *J. Mater. Sci. Lett.* **1999**, *18*, 1837−1839.
(19) Innocenzi, P.; Brusatin, G.; Babonneau, F. *Chem. Mater.* **2000**, *12*, 3726−3732.
(20) Hench, L. L.; West, J. K. *Chem. Rev.* **1990**, *90*, 33−72.
(21) Campo, M. A.; Babriel, D.; Kucera, P.; Gurny, R.; Lange, N. *Photochem. Photobiol.* **2007**, *83*, 958−965.
(22) Lovell, J. F.; Chen, J.; Liu, T. W. B.; Zheng, G. *Chem. Rev.* **2010**, *110*, 2839−2857.
(23) Skidmore, E. L; Powers, D. H. *Soil. Sci. Am. J.* **1982**, *46*, 1274−1279.
(24) Bonhomme, C.; Coelho, C.; Baccile, N.; Gervais, C.; Azaïs; Babonneau, F. *Acc. Chem. Res.* **2007**, *40*, 738−746.
(25) Peterson, J. *Minerals Eng.* **2010**, *23*, 504−510.
(26) Sysak, P. K.; Ching, T.-Y.; Foote, C. S. *Photochem. Photobiol.* **1977**, *26*, 19−27.
(27) Lindig, B. A.; Rodgers, M. A. J.; Schaap, A. P. *J. Am. Chem. Soc.* **1980**, *102*, 5590−5593.
(28) Di Mascio, P.; Sies, H. *J. Am. Chem. Soc.* **1989**, *111*, 2909−2914.

(29) Martinez, G. R.; Ravanat, J.-L.; Medeiros, M. H. G.; Cadet, J.; Di Mascio, P. *J. Am. Chem. Soc.* **2000**, *122*, 10212−10213.
(30) Aubry, J.-M.; Pierlot, C.; Rigaudy, J.; Schmidt, R. *Acc. Chem. Res.* **2003**, *36*, 668−675.
(31) Fudickar, W.; Linker, T. *Langmuir* **2010**, *26*, 4421−4428.
(32) Turro, N. J.; Ramamurthy, V.; Scaiano, J. C. In *Modern Molecular Photochemistry of Organic Molecules*; University Science Books: Sausalito, CA, 2010; pp 1001−1040.
(33) Toutchkine, A.; Aebisher, D. A.; Clennan, E. L. *J. Am. Chem. Soc.* **2001**, *123*, 4966−4973.
(34) Liu, F.; Fang, Y.; Chen, Y.; Liu, J. *J. Phys. Chem. B* **2011**, *115*, 9898−9909.
(35) Jensen, R. L.; Arnbjerg, J.; Ogilby, P. R. *J. Am. Chem. Soc.* **2010**, *132*, 8098−8105.
(36) Tromans, D. *Ind. Eng. Chem. Res.* **2000**, *39*, 805−812.
(37) Poling, B.; Prausnitz, J.; O'Connell, J. *The Properties of Gases and Liquids*; McGraw-Hill, New York, 2001.
(38) Levesque, F.; Seeberger, P. H. *Org. Lett.* **2011**, *13*, 5008−5011.
(39) Yavorskyy, A.; Shvydkiv, O.; Nolan, K.; Hoffmann, N.; Oelgemoller, M. *Tetrahedron Lett.* **2011**, *52*, 278−280.
(40) Maurya, R. A.; Park, C. P.; Kim, D.-P. *Beilstein J. Org. Chem.* **2011**, *7*, 1158−1163.
(41) Harper, J.; Sailor, M. J. *Langmuir* **1997**, *13*, 4652−4658.
(42) Fuchter, M. J.; Haffman, B. M.; Barrett, A. G. M. *J. Org. Chem.* **2006**, *71*, 724−729.
(43) Griesbeck, A. G.; Bartoschek, A.; Neudoerfl, J.; Miara, C. *Photochem. Photobiol.* **2006**, *82*, 1233−1240.
(44) Naito, K.; Tachikawa, T.; Cui, S.-C.; Sugimoto, A.; Fujisuka, M.; Majima, T. *J. Am. Chem. Soc.* **2006**, *128*, 16430−16431.
(45) Rossi, L. M.; Silva, P. R.; Vono, L. L. R.; Fernandes, A. U.; Tada, D. B.; Baptista, M. S. *Langmuir* **2008**, *24*, 12534−12538.
(46) Llansola Portolés, M. J.; Gara, P. M. D.; Kotler, M. L.; Bertolotti, S.; San Román, E.; Rodríguez, H. B.; Gonzalez, M. C. *Langmuir* **2010**, *26*, 10953−10960.
(47) Midden, W. R.; Wang, S. Y. *J. Am. Chem. Soc.* **1983**, *105*, 4129−4135.
(48) Sivaguru, J.; Solomon, M. R.; Poon, T.; Jockusch, S.; Bosio, S. G.; Adam, W.; Turro, N. J. *Acc. Chem. Res.* **2008**, *41*, 387−400.
(49) Wilkinson, F.; Helman, W. P.; Ross, A. B. *J. Phys. Chem. Ref. Data* **1995**, *24*, 663−1021.
(50) Bourne, R. A.; Han, X.; Poliakoff, M.; George, M. W. *Angew. Chem., Int. Ed.* **2009**, *48*, 5322−5325.
(51) Evans, D. F.; Upton, M. W. *J. Chem. Soc., Dalton Trans.* **1985**, *6*, 1141−1145.